Cell Reports
Sustainability

Article

Future soil organic carbon stocks in China under climate change

Graphical abstract

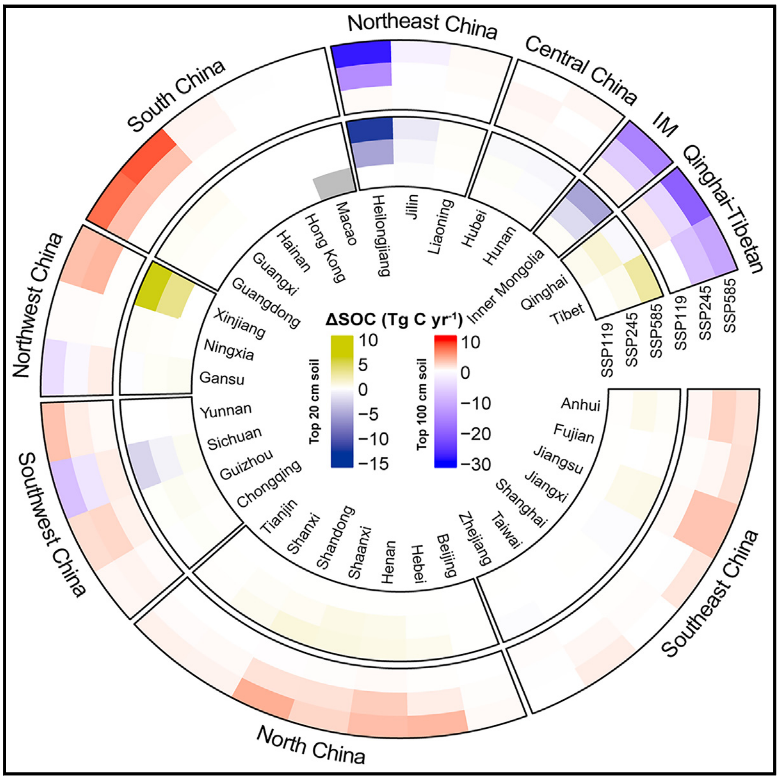

Authors

Jianzhao Wu, Shirong Liu, Changhui Peng, ..., Bing Wang, Zhouping Shangguan, Lei Deng

Correspondence

leideng@ms.iswc.ac.cn

In brief

Assessing future changes in China's soil organic carbon (SOC) is critical for achieving carbon neutrality. Using a comprehensive SOC database and climate-driven models, our projections for 2021–2100 reveal that under the sustainable SSP119 scenario, SOC will act as a carbon sink. Conversely, under SSP245 and SSP585, it may become a carbon source, underscoring the need for targeted soil conservation strategies.

Highlights

- Different methods yield significantly varied SOC estimates from the same dataset
- Top 1 m SOC was predicted to store 81.99 ± 1.90 to 88.92 ± 1.24 Pg C in China
- China's SOC in the top 1 m will function as a C sink under a low-emission scenario
- SOC loss hotspots shift to higher latitudes with increasing emissions scenarios

Wu et al., 2024, Cell Reports Sustainability *1*, 100179
September 27, 2024 © 2024 The Author(s). Published by Elsevier Inc.
https://doi.org/10.1016/j.crsus.2024.100179

CellPress

Cell Reports Sustainability

CellPress
OPEN ACCESS

Article

Future soil organic carbon stocks in China under climate change

Jianzhao Wu,[1] Shirong Liu,[2] Changhui Peng,[3,4] Yiqi Luo,[5] César Terrer,[6] Chao Yue,[1,7] Shouzhang Peng,[1,7] Jiwei Li,[1,7] Bing Wang,[1,7] Zhouping Shangguan,[1,7] and Lei Deng[1,7,8,*]

[1]State Key Laboratory for Soil Erosion and Dryland Farming on the Loess Plateau, Institute of Soil and Water Conservation, Northwest A&F University, Yangling, Shaanxi 712100, China
[2]Key Laboratory of Forest Ecology and Environment, China's National Forestry and Grassland Administration, Ecology and Nature Conservation Institute, Chinese Academy of Forestry, Beijing 100091, China
[3]Department of Biology Science, Institute of Environment Sciences, University of Quebec at Montreal, Montreal, QC H3C 3P8, Canada
[4]School of Geographic Sciences, Hunan Normal University, Changsha 410081, China
[5]School of Integrative Plant Science, Cornell University, Ithaca, NY 14853, USA
[6]Department of Civil and Environmental Engineering, Massachusetts Institute of Technology, Cambridge, MA 02139, USA
[7]Institute of Soil and Water Conservation, Chinese Academy of Sciences and Ministry of Water Resources, Yangling, Shaanxi 712100, China
[8]Lead contact
*Correspondence: leideng@ms.iswc.ac.cn
https://doi.org/10.1016/j.crsus.2024.100179

SCIENCE FOR SOCIETY China, the world's largest emitter of carbon dioxide (CO_2), has pledged to achieve carbon neutrality by 2060. Soils are the largest carbon pool in terrestrial ecosystems. Accordingly, carbon sequestration in soils is crucial for mitigating climate change, but the impact of various shared socioeconomic pathways on China's soil organic carbon (SOC) pool remains unclear. We anticipate that China's top 100 cm SOC will act as a carbon sink by 2100 under a sustainable development scenario. However, under intermediate and fossil fuel development scenarios, it will become a carbon source, indicating these scenarios do not favor soil carbon sequestration. This increases pressure on policymakers relying on soil to help reduce emissions. Our study shows that SOC in China will play a limited role in reaching carbon neutrality under future climate change. In the long run, only a reduction in CO_2 emissions will help to mitigate climate change.

SUMMARY

Quantifying soil organic carbon (SOC) is crucial for China's carbon neutrality goals, yet uncertainties exist due to future climate change. We compiled a comprehensive SOC database for China circa 2010 and utilized digital soil mapping methods to estimate SOC. Using a climate data-driven model, we projected SOC changes from 2021 to 2100 under different shared socioeconomic pathways (SSPs). The top 100 cm SOC is predicted to store 81.99 ± 1.90 to 88.92 ± 1.24 Pg C, with 37.8% to 41.7% in the top 20 cm. Under the SSP119 scenario, the top 100 cm SOC would increase by 11.5 ± 5.3 Tg C year^{-1}, contributing to 2.7% ± 1.6% of the carbon sink in China's terrestrial ecosystems over the same period. However, the top 100 cm SOC would transition into a carbon source under SSP245 and SSP585, despite geographical and provincial differences. Maps reveal SOC loss hotspots under SSP245 and SSP585, indicating priority regions for soil carbon conservation efforts.

INTRODUCTION

Carbon assumes a paramount role as the principal constituent of soil organic matter, serving as a linchpin in the maintenance of essential ecological functions. These functions encompass the regulation of biomass production, the preservation of soil and water integrity, the facilitation of nutrient cycling, and the conservation of biodiversity. The indispensability of carbon extends beyond its ecological contributions, as it emerges as a pivotal factor in climate-change mitigation and adaptation as well as a key enabler for the attainment of Sustainable Development Goals (SDGs).[1] On a global scale, an estimated 1,500 Pg C reside in the uppermost meter of soil, constituting a reservoir twice the magnitude of atmospheric carbon stocks and threefold that of biosphere carbon stocks.[2] Consequently, even minor fluctuations in soil organic carbon (SOC) stocks can lead to

© 2024 The Author(s). Published by Elsevier Inc.
This is an open access article under the CC BY-NC license (http://creativecommons.org/licenses/by-nc/4.0/).

significant impacts on atmospheric carbon dioxide (CO_2) concentrations.[3] Recognizing this, SOC dynamics have received a lot of attention at national, regional, and global scales.[4,5] Despite the attention, uncertainties persist due to variations in datasets and methodologies,[6] particularly in understanding the long-term spatial-temporal SOC dynamics anticipated under future climate-change scenarios.[1,7,8]

China has witnessed notable shifts in climate change over recent decades, a trend anticipated to persist until the end of the century.[9–11] Scholars have diligently investigated the size, distribution, and spatiotemporal changes of SOC stocks in China, employing inventory methods and various empirical or process models.[4,12,13] While these studies have predominantly focused on past SOC changes, there is a noticeable gap in research concerning the spatiotemporal changes of SOC under different future climate-change scenarios. A critical review of existing literature on future SOC changes underscores the absence of a simple, applicable, and rapid method to analyze these changes in China under diverse future climate scenarios. In predicting future SOC, the commonly used space-for-time approach warrants careful consideration, as it may introduce significant uncertainties when extrapolated beyond the climate-SOC space of the training set.[14,15] Moreover, previous research has tended to under-sample Western China, a region integral to China's terrestrial ecosystems and soil carbon sink.[4,16] The limited data from these under-sampled regions hinder precise SOC estimations for China's terrestrial ecosystems. This issue has been acknowledged in digital soil mapping (DSM) studies,[17,18] justifying the challenge of applying fully empirical space-time models due to the typically limited availability of soil data. Recognizing these challenges, there is a pressing need for a robust methodology to analyze the spatiotemporal changes of SOC in China under various future climate-change scenarios, particularly in under-sampled regions, to enhance our understanding of the country's soil carbon dynamics.

To address the modeling challenges outlined earlier, this study undertook the compilation and harmonization of the most comprehensive dataset of SOC stocks in terrestrial ecosystems across China circa 2010 (Figure 1). Employing self-developed climate data-driven models, we extended our efforts to generate prospective SOC maps for both the 0–20 and 0–100 cm soil layers in China, projecting from 2021 to 2100 under diverse climate-change scenarios. Additionally, we produced spatially explicit and nationally inclusive estimates of the predominant drivers influencing SOC dynamics within both soil layers. Our objectives encompassed: (1) advancing the comprehension of environmental drivers influencing SOC stocks in terrestrial ecosystems across China, specifically at the top 20 and 100 cm soil depths; (2) forecasting future alterations in China's SOC stocks under varying climate-change scenarios to identify conservation hotspots; and (3) mapping current and future SOC stocks, along with their associated uncertainties, under distinct climate-change scenarios across China at a spatial resolution of 1 km annually from 2021 to 2100. These findings aspire to provide insights that inform the development of nature-based climate-change mitigation strategies and support China's carbon neutrality goals.

RESULTS

Current SOC in China

We evaluated the performance of the six methodologies (ordinary kriging [OK], regression kriging [RK], regression tree [RT], random forest [RF], random forest plus kriging [RFOK], and forward feature selection with random forest [FFSRF]) incorporated in this study from three distinct perspectives: model performance evaluation (Figure S1; Table S1), model robustness (Figures S2 and S3), and spatial visualization inspection (Figures 2A, 2B, S4, and S5). The findings revealed the superior, or equivalent, efficacy of our developed FFSRF model that is predicated on the judicious selection of pivotal environmental covariates compared with the OK, RK, RT, RF, and RFOK methodologies.

The six methodologies employed in this study yielded comparable spatial patterns for both the top 20 cm SOC (hereafter SOC20) and the top 100 cm SOC (hereafter SOC100) across China, effectively capturing the principal spatial patterns and trends for SOC20 and SOC100, respectively (Figures 2A, 2B, and S4; Note S2). Furthermore, these methodologies accounted for 38% to 60% of the variation in SOC20 and 42% to 62% of the variation in SOC100 (Figure S1).

For SOC20, the estimated average SOC stocks across China around 2010 yielded by the six methodologies ranged from 33.5 ± 3.6 to 37.6 ± 2.5 Mg C ha^{-1} (Table S2). For SOC100, the estimated average SOC stocks across China around 2010 yielded by the six methods spanned 86.3 ± 2.0 to 93.6 ± 1.3 Mg C ha^{-1}. The total SOC100 over China in this period estimated by the six methods was 83.79 ± 4.85 (OK), 88.26 ± 3.14 (RK), 81.99 ± 1.90 (RT), 86.17 ± 0.95 (RF), 88.92 ± 1.24 (RFOK), and 83.98 ± 1.52 (FFSRF) Pg C. Of these values, 41.7%, 40.5%, 38.8%, 38.3%, 37.8%, and 39.5%, respectively, were stored in the top 20 cm soil (Figures 2C and 2D).

Changes in the SOC of China under future climate-change scenarios

China's SOC will exhibit fluctuating increasing or decreasing trends under different future climate-change scenarios (Figures 3A and 3B). Figure 3A illustrates that under the sustainable route scenario (shared socioeconomic pathway [SSP119]), China's SOC20 and SOC100 are projected to escalate by 4.29 ± 2.02 and 11.50 ± 5.35 Tg C $year^{-1}$, respectively, from 2021 to 2100. Under the intermediate route scenario (SSP245), China's SOC20 is projected not to exhibit a significant change trend. By contrast, China's SOC100 is projected to decline by 11.10 ± 4.19 Tg C $year^{-1}$. Conversely, under the fossil fuel development scenario (SSP585), both China's SOC20 and SOC100 are anticipated to decrease by 7.85 ± 1.84 and 40.90 ± 4.90 Tg C $year^{-1}$, respectively. Overall, the SOC dynamics in China are strongly dependent on the climate-change scenarios, with low-emission scenarios leading to SOC accumulation and high-emission scenarios resulting in SOC loss.

Figure 3C illustrates the spatiotemporal trends of SOC in China under diverse future climate-change scenarios. The findings suggest that the response of SOC to climate change will intensify as greenhouse gas (GHG) emissions escalate. Notably, regions with abundant SOC, such as the forest and wetland ecosystems

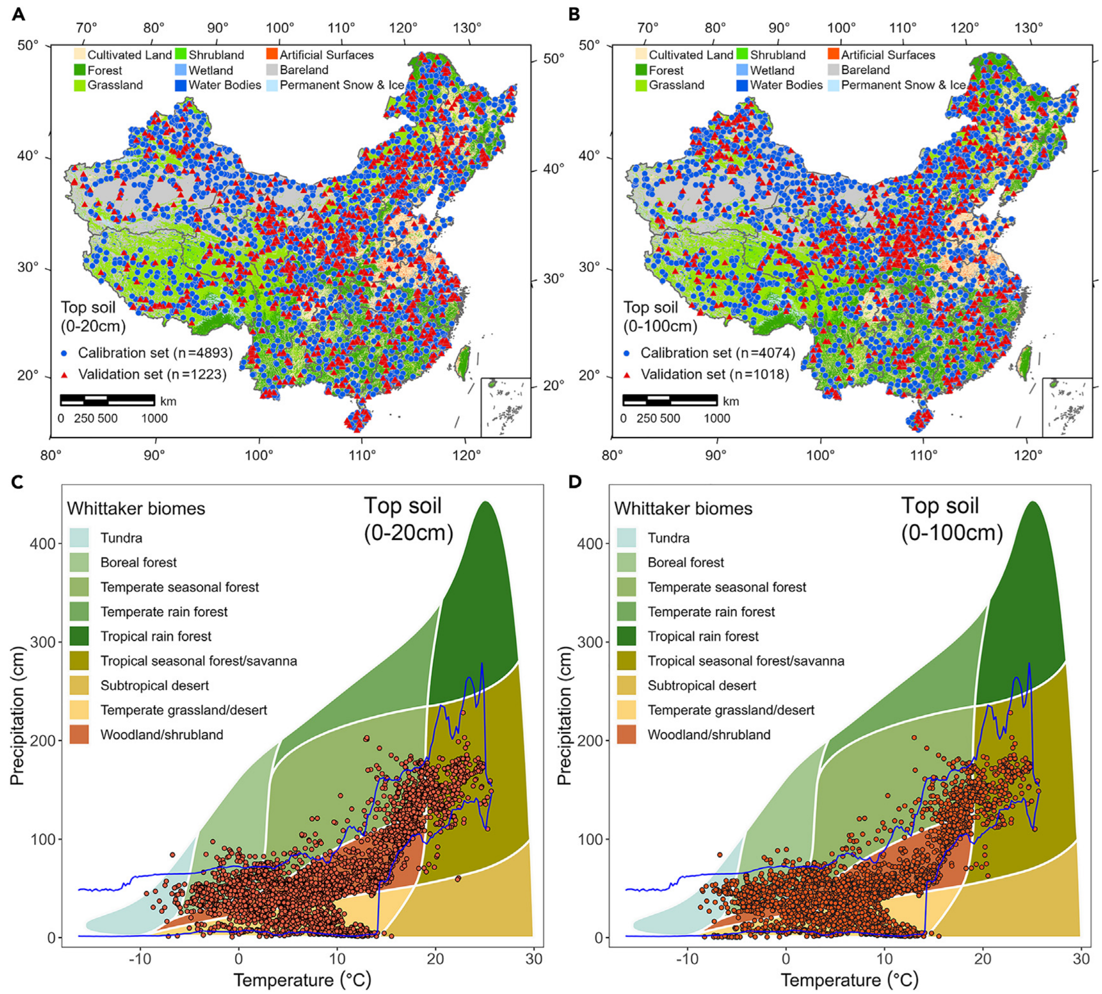

Figure 1. Spatial distribution of sample sites

(A–D) Distribution of the SOC sampling sites with data used in this study for (A) top 20 cm soil and (B) top 100 cm soil. The base map is based on GLOBALLAND30 data in 2010 (http://www.globallandcover.com/). The distribution of site-level training data is based on Whittaker biomes[19] for (C) top 20 cm soil and (D) top 100 cm soil. The blue line represents the 95% confidence interval of the mean annual precipitation (MAP) change in Chinese territory with respect to the mean annual temperature (MAT).

in the Northeast and the alpine meadow and wetland regions on the Tibetan Plateau, appear more vulnerable to SOC loss due to climate change. However, North China, South China, and Xinjiang Province are predicted to emerge as hotspots for SOC sequestration under the SSP245 and SSP585 scenarios, with sizable SOC accrual by 2060. Moreover, our findings reveal an intriguing trend in which the primary region of noticeable SOC loss in both soil strata appears to migrate toward higher latitudes with escalating GHG emissions (from SSP119 to SSP245 to SSP585; Figures 3C and 3D). Besides, Figure S6 delineates that under both SSP245 and SSP585, regions in China with mean annual temperatures (Temp) oscillating between $-10^{\circ}C$ and $4^{\circ}C$ are anticipated to transform into significant hotspots for SOC emissions.

We evaluated the trend of SOC in each province in China from 2021 to 2100 under different climate-change scenarios (Figure 4; Table S3; Figures S7 and S8), and we only considered the region of significant change (i.e., $p < 0.05$) in the pixel-by-pixel linear regression from 2021 to 2100. Figures 4A–4F present three key findings. First, under the SSP119 scenario, the vast majority of Chinese provinces function as SOC sinks. However, under the SSP245 and SSP585 scenarios, the Heilongjiang, Inner Mongolia, Qinghai, Tibet, and Sichuan provinces transition into carbon sources. Second, the rates of SOC increase or decrease is most pronounced under the SSP585 scenario across all provinces. Third, in terms of SOC100, provinces such as Heilongjiang, Inner Mongolia, Tibet, Qinghai, and Sichuan emerge as hotspots for SOC loss under the SSP245 and SSP585 scenarios. Conversely, provinces including Xinjiang, Guangxi, Guangdong, Shandong, Henan, Jiangsu, Anhui, Shaanxi, Guizhou, and Hebei become hotspots for SOC sequestration.

China's nine geographic divisions are predicted to continue to exhibit high spatial heterogeneity in terms of their potential as carbon sinks/sources under future climate-change scenarios.

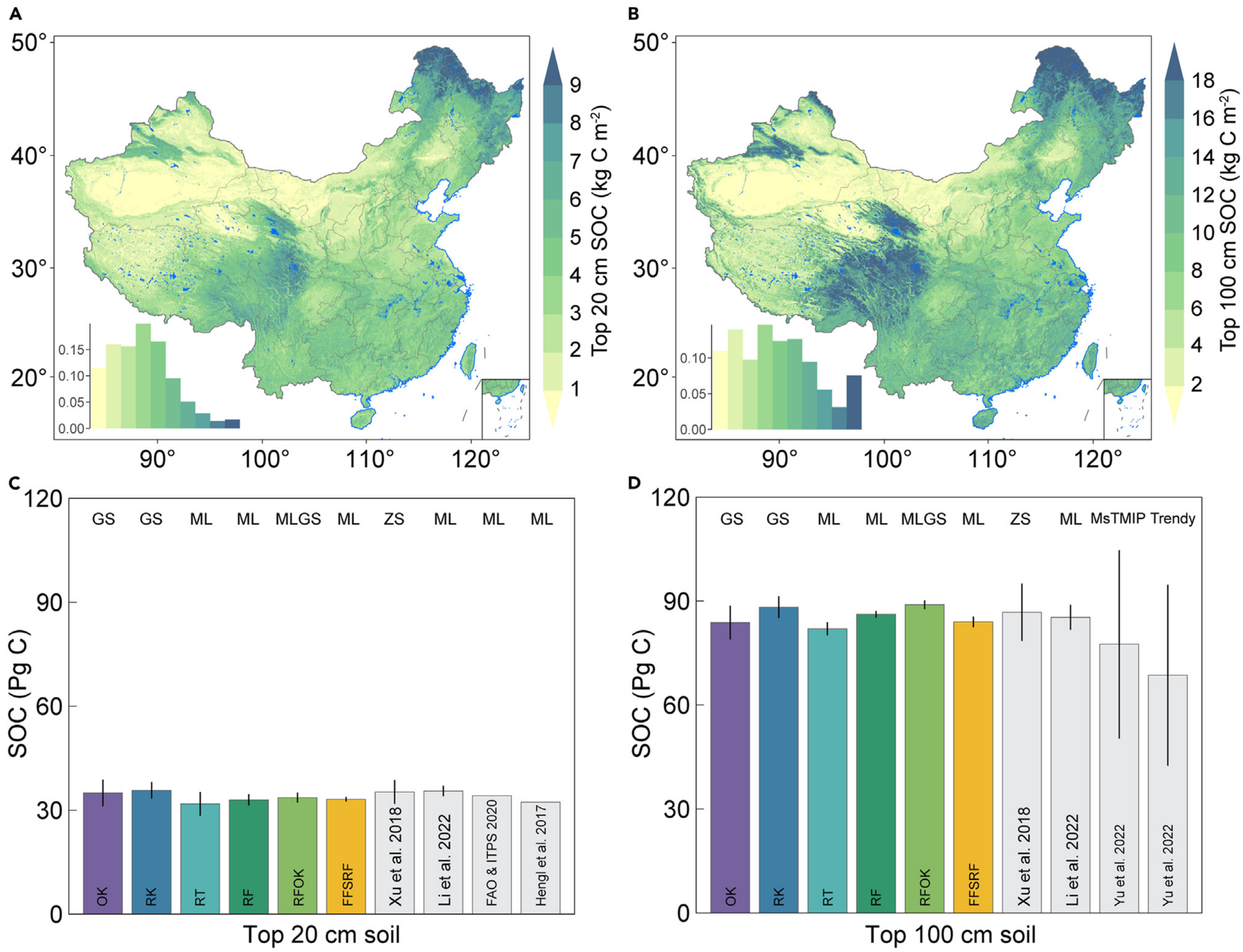

Figure 2. Spatial distribution and magnitude of SOC in China around 2010

Using the coupled forward feature selection and random forest method.

(A) Illustrates the spatial distribution of SOC in the top 20 cm soil across China.

(B) Depicts the spatial distribution of SOC in the top 100 cm soil across China. The inset in the bottom-left corner is a probability density distribution plot.

(C) Presents the magnitude of China's SOC derived from different methodologies and literature. OK, ordinary kriging; RK, regression kriging; RT, regression tree; RF, random forest; RFOK, random forest plus kriging; and FFSRF, forward feature selection coupled with random forest. The gray bars represent previous literature, i.e., Xu et al.,[16] Li et al.,[4] FAO and ITPS 2020,[1] Hengl et al.,[7] and Yu et al..[20] GS, geostatistics; ML, machine learning; MLGS, the integration of machine learning and geostatistics; ZS, zonal statistics; MsTMIP, Multiscale Synthesis and Terrestrial Model Intercomparison Project (https://daac.ornl.gov/cgi-bin/dsviewer.pl?ds_id=1225); and Trendy, the trends in the land carbon cycle project (https://blogs.exeter.ac.uk/trendy/). The error bars denote the standard deviation. The gray line denotes the provincial boundary. The blue scattered patches are water bodies.

However, certain deterministic patterns emerged (Figure 4G). For instance, in the top 20 cm soil, SOC sequestration rates in North China, South China, the Tibetan Plateau, and Northwest China will tend to increase in response to escalating GHG emissions. By contrast, Northeast China and Inner Mongolia are likely to experience heightened SOC loss rates in the transition from the SSP245 to the SSP585 scenario. However, when examining the top 100 cm soil, a distinct pattern emerges. While increased SOC sequestration rates are projected in South China, North China, and Southeast China with rising GHG emissions, Northeast China, Inner Mongolia, and the Tibetan Plateau are set to become hotspots for SOC loss. Notably, this trend is expected to intensify in line with GHG emissions.

In summary, our findings illustrate a spatial offset effect of climate change on SOC alterations in China. This implies that climate change can either augment or diminish SOC in different regions, highlighting the regionally diverse impacts of climate change on SOC dynamics.

DISCUSSION

In an effort to affirm the efficacy of the FFSRF methodology, it was compared with five of the most prevalent DSM techniques (OK, RK, RT, RF, and RFOK). Our comparative analysis revealed that our FFSRF approach consistently achieved prediction accuracies that were either superior or equivalent to those of the other

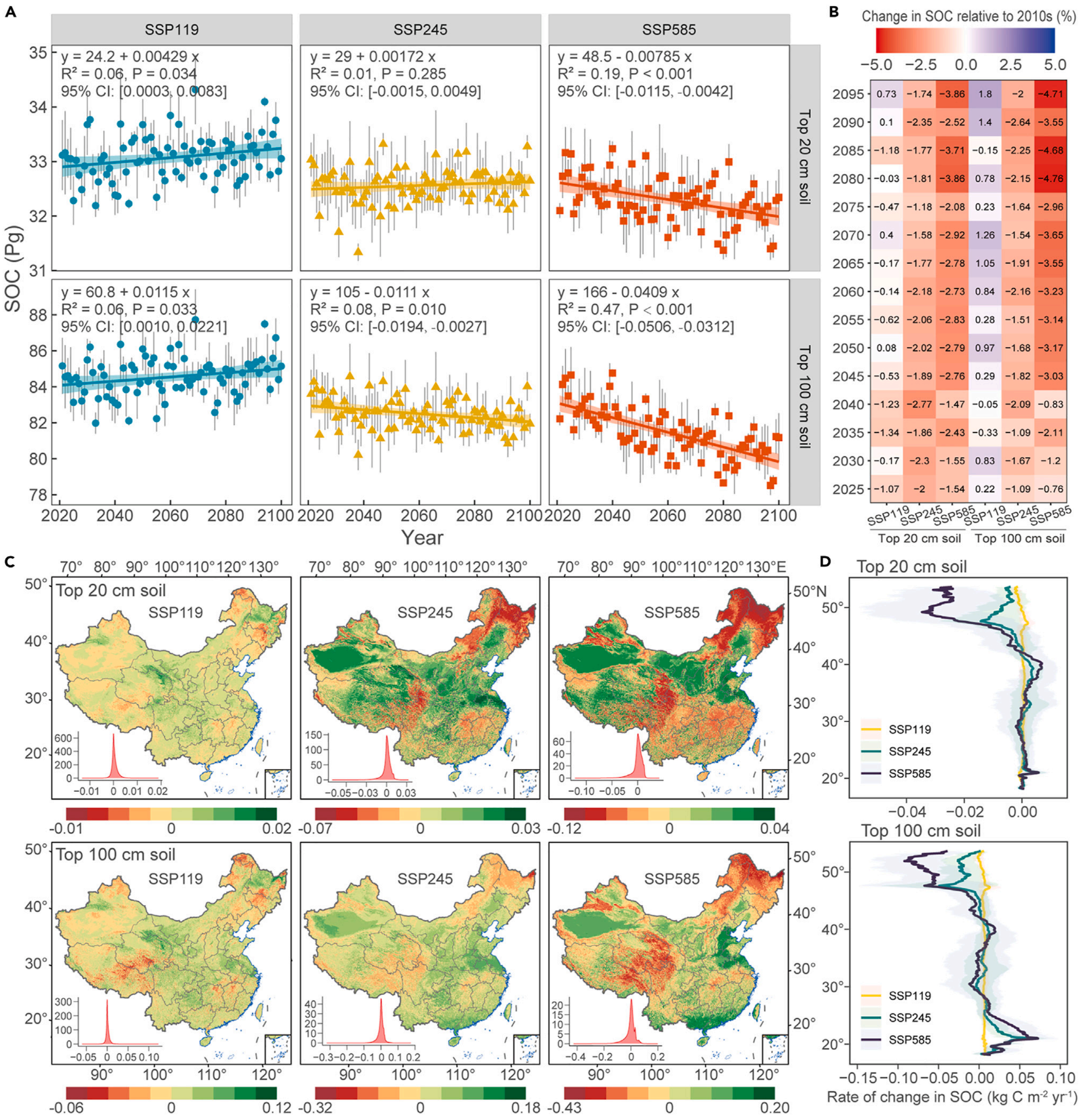

Figure 3. Trends of SOC in China from 2021 to 2100 under different future climate-change scenarios

(A) Delineates the trajectory of SOC changes (Pg C year^{-1}) in China under these scenarios, with 95% confidence intervals represented by shaded areas.

(B) Shows the relative SOC changes compared with the 2010s.

(C) Maps the spatial distribution of the annual average changes of SOC (kg C m^{-2} year^{-1}; 1 kg C m^{-2} year^{-1} = 10 Mg C ha^{-1} year^{-1}) in China under different future climate scenarios, and their coefficients of determination (R^2) and significance (p value) can be found in Figures S7 and S8. The inset in the bottom-left corner represents the corresponding probability density distribution.

(D) Presents the latitudinal statistics of the annual average changes of SOC (kg C m^{-2} year^{-1}), with the shaded area indicating the standard deviation. We provide plots of the probability density distributions of historical training climate variables and future projected climate variables (Figures S32–S34). We can see that our predictions mostly remained within the observed historic training data climate space. For the three SSPs under the three ESMs, the area outside the climatic range of the training set accounted for less than 1%. In addition, we also report the individual ESM-based results for comparison (Figure S35).

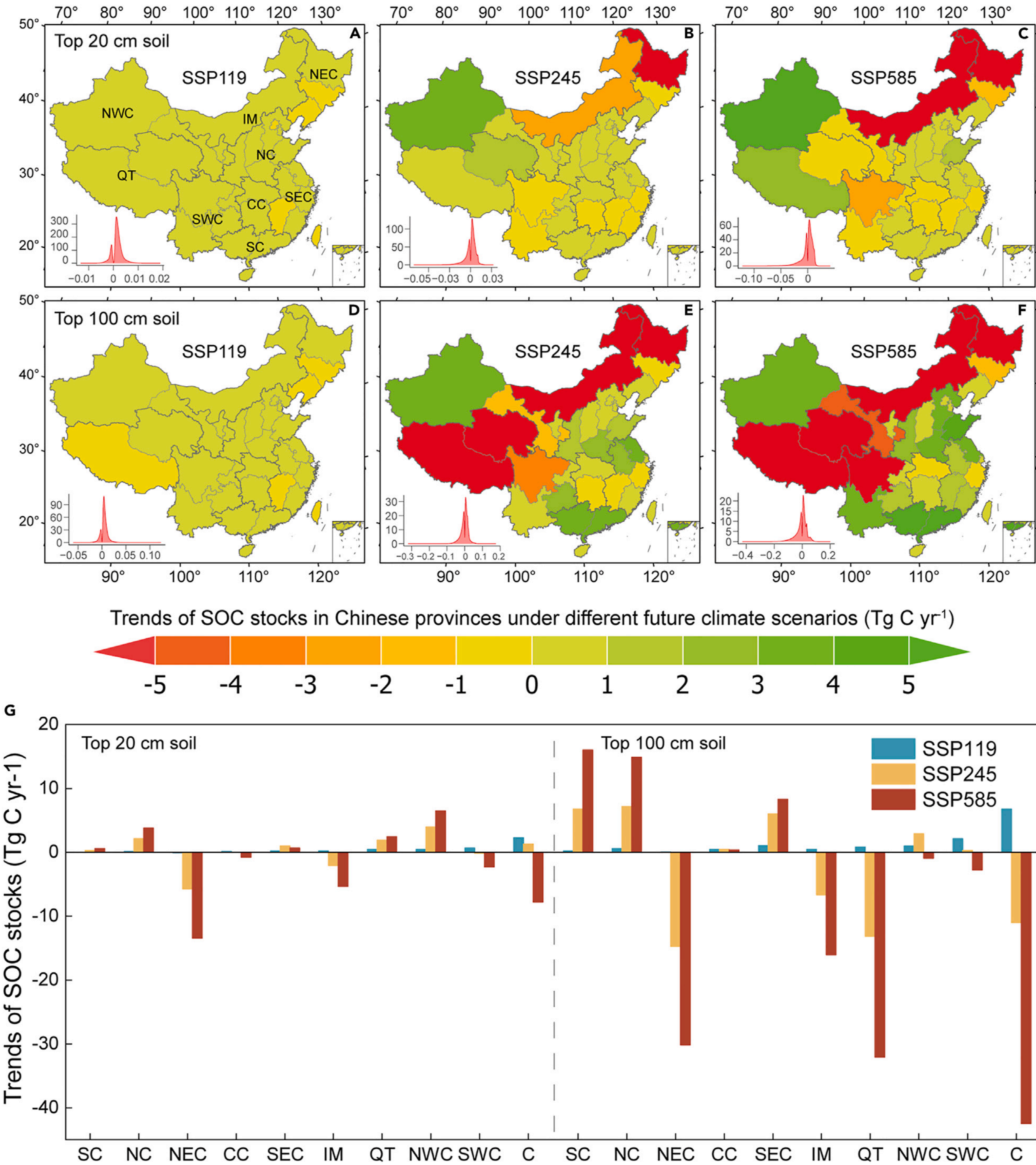

Figure 4. Trends of provincial-scale SOC stocks (Tg C year^{-1}) in China under different future climate-change scenarios

(A–C) Illustrate the trends of top 20 cm SOC changes across provinces under different future climate-change scenarios.

(D–F) Illustrate the trends of top 100 cm SOC changes across provinces under different future climate-change scenarios.

(G) Illustrates the trends of SOC changes across different geographical regions under different future climate-change scenarios. The nine sub-regions are SC, South China; NC, North China; NEC, Northeast China; CC, Central China; SEC, Southeast China; IM, Inner Mongolia; QT, Qinghai-Tibetan; NWC, Northwest China; and SWC, Southwest China. (C) indicates the entire country. The bottom-left insets in (A)–(F) represent the respective probability density plots. Note that we only considered the region of significant change (i.e., $p < 0.05$) in the pixel-by-pixel linear regression (from 2021 to 2100). Further details are provided in Table S3.

five methods (Figure S1; Table S1). This approach, which is predicated on a precisely chosen set of key environmental variables, exhibited robustness in its predictions. In addition, for the first time, we compared traditional geostatistical methods with recently popularized machine learning techniques at a sub-continental scale. Our findings indicate that assessing the performance of models based solely on predictive accuracy is insufficient. Machine learning did not significantly improve the model's R^2 or ρ_c, nor did it substantially reduce the root mean square deviation (RMSE) or mean error (ME) (Figure S1). This highlights the need for a comprehensive evaluation of model performance, which encompasses traditional predictive accuracy metrics, model robustness, and spatial visualization checks.

Concerning the estimation of SOC stock, we found that the top 100 cm SOC stock in China around 2010 ranged from 81.99 ± 1.90 to 88.92 ± 1.24 Pg C, as calculated using the six methodologies. Among them, 37.8% to 41.7% were stored in the top 20 cm. Interestingly, nearly all prior estimates align within this range[4,16,21] (Table S2), underscoring the notion that even when working with identical datasets, the disparities in estimations across different methodologies should not be dismissed. Yet, it is worth noting that two prevalent multi-model integrated comparison projects (MsTMIP and Trendy; Figures 2C and 2D), which are based on process models, tend to underestimate the SOC stock in the top 100 cm soil across China.

To further validate our estimates, comparison of the estimates with two global datasets (GSOCmap v.1.5.0 and SoilGrids 250 m v.2.0) revealed that both underestimated the SOC of the top 20 cm soil in China (Figure S5). Yet, several studies found that SoilGrids 250 m v.2.0 overestimated the SOC of the top 100 cm soil in China.[4,22] Accordingly, Li et al.[4] examined the global soil profiles used to generate subsoil SOC maps (under 15 cm) in SoilGrids and discovered there are only 2,886 sites spread across China, which only represent 1.52% of all global subsoil sites. SoilGrids SOC maps were generated by a global-scale model trained from these global observations.[7] We inferred that this phenomenon may be because the average SOC of the global top 20 cm soil is lower than that of China, but the average SOC of the global top 100 cm soil is higher than that of China. Training the model with global-scale data resulted in this difference (Figure S5).

Concerning the spatial distribution of SOC20 and SOC100 in China, all six methods showed similar spatial patterns, capturing the main spatial trends and patterns of SOC20 and SOC100, but the extreme SOC values ranges varied significantly (Figure S4). The estimated SOC20 and SOC100 showed an overall similar spatial pattern with the GSOCmap v.1.5.0 and SoilGrids 250 m v.2.0 (Figure S5) and other studies.[4,21,23]

The issue of the pronounced uncertainty in under-sampled regions, which is a concern that has been consistently highlighted in previous studies,[7,8,13] has been significantly mitigated in our study (Figures S9 and S10). This notable improvement is largely attributable to the use of an unprecedented database of Chinese SOC sample sites around 2010. Furthermore, the distribution of high-uncertainty areas in our SOC maps coincides with areas of high SOC. This finding is instructive for the strategic placement of future SOC sample sites, suggesting an increased focus on areas with high SOC values.

To affirm the model's proficiency in predicting the temporal dynamics of China's SOC, we scrutinized the ability of the FFSRF methodology to trace the progression of SOC changes in China over time. Our examination involved utilizing data from the Second Soil Survey of China (1978–1984) to evaluate the performance of the FFSRF. The analysis revealed that the FFSRF could account for 45% of the variability in Chinese SOC during the 1980s (Figure S11). This demonstrates the model's proficiency in reproducing SOC trajectories. Capitalizing on the proven capability of FFSRF, we coupled it with climate projections from three Earth system models to forecast potential SOC shifts in China from 2021 to 2100 under different climate scenarios.

Our findings indicate a projected increase in future SOC within China under SSP119 (Figure 3), which aligns with the trend observed in the 16 Earth system models ensemble averages from CMIP5 for simulated SOC changes in China under the same scenario.[24] Conversely, under SSP245 and SSP585, we anticipate a decrease in China's future SOC, with the decline being more pronounced under SSP585. We elected to visually represent and analyze the SOC projections under SSP585 utilizing four Earth system models from CMIP6 (Figure S12). Our results are considerably consistent with the SOC trends predicted by the EC-Earth3-veg model across most of the region. Furthermore, we observed a decrease in SOC100 under SSP245, while no significant trend was detected in SOC20. This could be attributed to the heightened sensitivity of subsoil organic matter to Temp changes, where warming may result in the loss of younger, fresher, and more readily available organic matter, leaving behind a higher proportion of more stable organic matter.[25] Our findings highlight that under SSP245 and SSP585 (incl. changes in Temp and precipitation [Pre] regimes), the top 100 cm soil across China would be a source of carbon.

In addition, the anticipated annual carbon increment in SOC100 under SSP119 across China, considering only the region of significant change (i.e., $p < 0.05$) in the pixel-level linear regression from the decade beginning in 2021 to 2100, equates to approximately 0.4% of China's anthropogenic emissions concurrently.[26] In the past 2 decades, many methods have been used to estimate terrestrial carbon sinks in China. These studies suggest that terrestrial ecosystems in China are an important carbon sink, but there are discrepancies in the estimates from different methods (ranged from 0.177 to 1.11 Pg C year^{-1}).[26–30] Assuming that the size of the Chinese terrestrial ecosystem carbon sink remains within this range in the future, the losses of SOC in the top 100 cm under SSP245 and SSP585 would offset 1.0% to 6.3% and 3.7% to 23.1% of the sink, respectively.

Recently, Xu et al.[31] estimated Chinese terrestrial carbon sinks for 2010–2060, finding no significant differences between SSPs, averaging 0.42 ± 0.02 Pg C year^{-1} during this period. According to Xu et al.,[31] under the SSP119 scenario, the top 100 cm SOC in China would increase by 11.5 ± 5.3 Tg C year^{-1}, contributing to 2.7% ± 1.6% of the carbon sink in China's terrestrial ecosystems over the same period. By contrast, under the SSP245 and SSP585 scenarios, the top 100 cm SOC in China was anticipated to counterbalance 2.6% ± 1.0% and 9.7% ± 1.2% of China's terrestrial ecosystems carbon sink, respectively.

Intriguingly, the primary region of discernible SOC diminution in the two soil strata appears to shift northward along the latitude in correlation with an escalation in GHG emissions, progressing from SSP119 to SSP245 to SSP585. This observation may be corroborated by two recent studies. One study posited that climate change instigates the migration of core microorganisms, which tend to gravitate northward under climate-change scenarios, thereby mediating the global succession of soil attributes.[32] The second study suggests that prolonged thermal acclimatization of soil microorganisms in low-latitude forests results in decreased soil carbon emissions.[33]

Our results show that the area of Pre-dominated SOC change for the two soil layers would decrease with escalating GHG emission scenarios but that Pre and Temp co-dominance and Temp dominance would increase in almost all nine geographic subdivisions and nationwide (Figure S13; Note S2). This may be due to the more pronounced relative changes in Temp compared with Pre as GHG emissions intensify. To eliminate the confounding impacts of Temp and Pre and to more precisely elucidate the relationship between either Temp or Pre and SOC, partial correlation analyses were performed. As depicted in Figure S14, annual Pre is positively correlated with SOC in over 75% of the regions across China. Conversely, annual Pre is negatively correlated with SOC in South China and Southeast China.

Overall, our results highlight the variability of carbon-climate feedback in the different regions of China. For example, northern China would be a carbon sink (negative feedback). By contrast, northeastern China would be a carbon source (positive feedback). Given that soil has traditionally functioned as a carbon sink, the potential impact of future climate change could inhibit its capacity to provide this essential ecosystem service (carbon sequestration). Consequently, to meet CO_2 emission reduction targets and avert the realization of the SSP585 scenario, further reduction in permissible emissions from human activities is necessary.

Our findings underscore the pressing necessity for governmental interventions aimed at enhancing the capacity for SOC sequestration in areas exhibiting a decline in SOC, thereby fostering an increase in SOC storage. Consequently, the formulation of efficacious soil-based mitigation strategies should be underpinned by comprehensive strategic assessments. Detailed local or regional knowledge should be incorporated by tailoring land management to more effectively meet local/regional requirements. Irrespective of the soil management practices adopted, a reliable and detailed evaluation of SOC is indispensable. Our maps offer measurements of SOC change in China under future climate-change scenarios and a crucial mechanism to steer targeted soil-based restoration interventions based on geographical location. The results accentuate the need to adopt integrated perspectives and consider regional differences in nature-based solutions. There are significant implications for the realization of China's carbon neutrality goals by 2060.

The spatial mapping of SOC also signifies a growing requirement for spatially explicit SOC assessments for various applications, such as prioritizing local actions in soil carbon sequestration and monitoring temporal changes in SOC. Additionally, SOC maps serve as valuable inputs for Earth system models and are pertinent for calibrating and initializing mechanistic simulation models of the terrestrial carbon cycle.

Limitations

There are several limitations/uncertainties in our climate-driven approach. First, it is a space-for-time substitution approach. This does not the assessment of the effects of other global change factors that may accompany climate change, such as elevated CO_2, nitrogen deposition, and fire. Although we estimated long-term steady-state trends in SOC under climate-change scenarios and not transient unstable states, the results would likely overestimate the loss of SOC when considering the general positive effects of elevated CO_2 and N deposition on plant growth.[34–36] Second, the potential effects of changes in other climatic variables, such as extreme climate events, which may interact with changes in Temp and Pre regimes to determine the net balance of SOC[37,38] were not considered. Third, our projections are based on future climate-change scenario data from three Earth system models (EC-Earth3, GFDL-ESM4, and MRI-ESM2-0).[11,39] Therefore, the predictions may contain certain uncertainty arising from the uncertainty associated with these datasets and the models that generated them. Further research is needed to address these limitations.

EXPERIMENTAL PROCEDURES

Resource availability

Lead contact

Further information and requests for resources and reagents should be directed to and will be fulfilled by the lead contact, Lei Deng (leideng@ms.iswc.ac.cn).

Materials availability

This study did not generate new, unique reagents.

Data and code availability

The original Chinses SOC inventory is from the studies.[16,40–42] This paper does not report original code. All data presented and computer codes used in this study are available in the supplemental information and also from the lead contact upon reasonable request. Any additional information required to reanalyze the data reported in this paper is available from the lead contact upon request.

SOC stock data

We reconstructed the SOC stock database in China around 2010 for the top 20 cm and top 100 cm soil. This updated database represents the most extensive and inclusive collection of SOC data in China to date, representing all of China's terrestrial ecosystems, soil types, and land uses (Figure 1). Our new updated database builds on that of a previous study[16] by supplementing the dataset with samples from sparse sample area or sampling gaps, especially in the arid zones of China, Tibetan Plateau, and Xinjiang Province, which also tended to be missing or underrepresented areas of sample sites in previous studies.[4,13,21,43] Specifically, a publicly available SOC dataset[16] includes 4,536 samples from the top 20 cm of soil and 3,147 samples from the top 100 cm of soil across China between 2004 and 2014, collected from *in situ* investigations of 1,036 publicly available papers and databases.

The new data come from two sources. First, from 2009 to 2011, to fill the soil sampling gap, our collaborators conducted an extensive survey of SOC in China, particularly in the arid and semi-arid regions of Western China. Soil samples were collected to measure soil texture, bulk density, and organic carbon at depth intervals of 0–20 and 0–100 cm using a soil auger. Within each depth interval, at least five samples from plots were collected along diagonal lines. Altogether, 1,580 soil samples were collected from terrestrial ecosystems in China. The SOC content was measured using the potassium dichromate heating method[44] (i.e., Walkley-Black wet digestion method). Second, by further filling the soil sampling gaps, we obtained 367 soil samples, comprising 114 soil samples from permafrost zones of the Qinghai-Tibetan Plateau[40]), 201 samples from permafrost zones of the Qinghai-Tibetan Plateau,[41] and 52 sail samples from dryland in China.[42] Altogether, the updated dataset comprised 6,116 top 20 cm soil samples and 5,092 top 100 cm soil samples (Figure 1; Table S4). All samples collected from China were widely distributed, spanning the major ecosystems of China. We used a similar approach to that previously described.[18,45] SOC stock for each layer from the different datasets was calculated as:

$$SOC\ density\ \left(kg\ C\ m^{-2}\right) = OC \times BD \times D \times (1 - g) \times 0.1 \qquad \text{(Equation 1)}$$

where OC is the SOC content (%), BD is the bulk density (g cm^{-3}), D is soil depth (cm), and *g* is the gravimetric proportion of gravel (>2 mm) in the sample.

We divided the sample points for SOC20 and SOC100 into two groups, respectively. Eighty percent of the sample points (n = 4,893 for SOC20; n = 4,074 for SOC100) were used to calibrate the model, while 20% (n = 1,223 for SOC20; n = 1,018 for SOC100) were used to validate the model. Both partitions were done randomly by using the "create subset" function of geostatistical analyst in ArcGIS Pro 3.1. Table S4 presents the summary statistics of the calibration and validation sets for SOC20, SOC100, and their logarithmic conversions. We performed log-transformation to address the high positive skewness in the distribution of SOC. To avoid negative values, we used Ln (SOC+1). Further analyses were performed on the log-transformed data. The predicted SOC values were back-transformed to their original scale to facilitate interpretations.

Environmental covariates

The amount, distribution, and duration of SOC in a given ecosystem are controlled by environmental factors such as climate, soil texture, parent material, topography, and organisms over time. This concept was initially presented in a prior study[46] and subsequently generalized and formalized as the SCORPAN model[47] (Note S1). This model has become the foundation for contemporary DSM. Following SCORPAN, we selected the environmental covariates associated with these factors and processes. Redundant environmental variables[4,48] were removed if their Pearson correlation coefficients with other variables were >0.9. Tables S5 and S6 list the covariates used for SOC spatial prediction in this study, grouped by the soil-forming factor each represents.

Five groups of covariates were considered for use in predictive soil mapping. The first was climate-related covariates, including average annual Temp, annual Pre, and annual potential evapotranspiration (Pet). The second was vegetation and living organisms, including the fraction of absorbed photosynthetically active radiation (FAPAR), normalized difference vegetation index (NDVI), enhanced vegetation index (EVI), net primary productivity (NPP), aboveground biomass (AGB), belowground biomass (BGB), leaf area index (LAI), and land cover types (LC). The third was relief and topography-related covariates, including digital elevation model (DEM), slope, aspect, plan curvature (PLC), profile curvature (PRC), landform classes (LFCs), topographic wetness index (TWI), and vertical distance channel network (VDCN). The fourth was parent material/geologic material covariates, including lithology (Li) and depth to bedrock (DTB). The fifth was soil-related covariates, including soil orders (SOs; FAO-90), clay content (clay), sand content (sand), silt content (silt), groundwater table depth (WTD), average soil and sedimentary deposit thicknesses (SSDTs), and drainage classes (drainage). More information about the environmental covariates, such as the definition and description of each environmental covariate, data source, and resolution, is in Tables S5 and S6 and Note S1.

Prior to fitting spatial prediction models and generating soil maps, we prepared covariate layers that represent independent variables (i.e., predictor variables) in statistical modeling (see Note S1 for details). The main processing steps included: (1) conversion of polygon maps to rasters, (2) reprojection of data to coordinate system lon/lat WGS84 using the nearest neighbor method (where necessary), (3) resampling data to 30 arcsec grid (1,000 m) resolution using the nearest neighbor method (note that we only use the scale-up method, i.e., upscaling (aggregating) raster to match the target resolution (1,000 m), where necessary), and (4) filling NoData values in the vicinity of the national boundary line (in case the environmental covariates did not use the proposed empty grid range) using an inverse distance weighting algorithm.

Exploratory analyses

We explored the bivariate relationship between SOC20 and SOC100 at paired positions (i.e., with identical coordinates; Figure S15; Note S2). All the bivariate relationships except those in others for LC types due to the small sample size and the inclusion of multiple ecosystem types, such as bare land, wasteland, and sandy land, were fitted with linear regression.

The main objective of the statistical analysis was to explore the relationship between SOC and different predictor variables. Statistical analysis was performed using R (version 4.1.2, R Core Team).[49] In the first step, the individual impacts of LC, SO, LFC, Li, drainage, and aspect on SOC density (for categorical predictor variables; Figures S16–S21; Note S2) were evaluated. The bivariate relationships between the SOC and sites properties (for continuous predictor variables; Figures S22–S25; Note S2) were explored. The categorical predictor variables were used as dummy variables to separately perform linear regressions with SOC (Table S7). Subsequently, Pearson correlation analyses for all continuous variables were performed (Figure S26). Multivariate stepwise regression based on the Akaike information criterion was also performed to identify significant environmental variables that affect SOC. The respective explanatory power of the SCORPAN factors was quantified using a variance decomposition model (Figure S27). These simple methods did not work well (Note S2), perhaps due to not accounting for the complicated interactions of the regime associated with SCORPAN on SOC and the spatial autocorrelation of SOC (Tables S8 and S9). We used more comprehensive methods (e.g., RF) to predict SOC.

Methodology for estimating current SOC

Five widely used DSM methods were selected: OK, RK, RT, RF, and RFOK. Further details on these methods are available elsewhere[4,50,51] (Note S1). Modeling, analysis, and mapping of the above methods were performed in R (R Core Team)[49] and ArcGIS Pro 3.1.

SOC mapping accuracy was evaluated using an independent validation dataset, which is more rigorous than the common cross-validation approach.[52] The same training and validation datasets were applied to all methods, thus avoiding errors due to random sampling and enhancing comparability between methods. The SOC values for the validation sites were derived from the predicted SOC maps. Four metrics—ME, root mean square error (RMSE), coefficient of determination (R^2 value), and Lin's concordance correlation coefficient (ρ_c)[53] were used to evaluate the performance of the different methods. A good prediction usually has high R^2 and ρ_c and low ME and RMSE value. The formulas of ME, RMSE, R^2, and ρ_c are as follows in Equations 2, 3, 4, and 5):

$$ME = \frac{1}{n}\sum_{i=1}^{n}\left(pred_i - obs_i\right) \qquad \text{(Equation 2)}$$

$$RMSE = \left(\frac{1}{n}\sum_{i=1}^{n}\left(obs_i - pred_i\right)^2\right)^{\frac{1}{2}} \qquad \text{(Equation 3)}$$

$$R^2 = 1 - \frac{\sum_{i=1}^{n}\left(obs_i - pred_i\right)^2}{\sum_{i=1}^{n}\left(obs_i - \overline{obs}\right)^2} \qquad \text{(Equation 4)}$$

$$\rho_c = \frac{2\rho\sigma_{pred}\sigma_{obs}}{\sigma_{pred}^2 + \sigma_{obs}^2 + \left(\mu_{pred} - \mu_{obs}\right)^2} \qquad \text{(Equation 5)}$$

where *obs* is the observed SOC, *pred* is the predicted SOC from a given model, n is the number of validation sites i, $\overline{obs}$ is the average value of observed SOC, ρ is the correlation coefficient between the predictions and observations, μ_{pred} and μ_{obs} are the means of the predicted and observed values, respectively, and σ^2_{pred} and σ^2_{obs} are the corresponding variances. The statistic evaluates both imprecision and bias.

The performance assessment indices varied with the methods that were compared (Figures S1 and S28). Detailed information on the performance of these methods is provided in Figure S2. In addition, the predicted spatial distribution of SOC was evaluated by comparing it with the widely used global SOC grid data (i.e., SoilGrids250m and GSOCmap v1.5.0). As well, the magnitude of our estimated SOC across China was compared with previous studies[4,16,20,21,43] (Table S2).

Three distinct approaches were used to estimate the uncertainty in predicting SOC. Initially, when the prediction methodology incorporated a formal uncertainty analysis, the provided uncertainty estimates were utilized. Subsequently, for independent SOC estimates derived from disparate methods, the standard deviation of these independent estimates was reported as the uncertainty between methods. Lastly, in the case of RF, the predictive uncertainty of SOC was evaluated by the bootstrap method. Specifically, the standard deviation of 30 bootstrap iterations was computed to quantify the uncertainty.

The uncertainties in SOC estimations among the five methods suggested that the high uncertainties were primarily located in mountainous regions for the two soil layers, such as along the Tibetan Plateau, Northeast, and Tien Shan. These areas are characterized by high SOC levels or complex and variable local landscapes (Figure S9). On an aggregate level, the nationally averaged uncertainties for SOC20 and SOC100 were 3.6 and 5.9 Mg C ha^{-1}, respectively. However, when considering the RF model exclusively, the nationally averaged uncertainties for both SOC20 and SOC100 were notably diminished to 1.6 and 4.1 Mg C ha^{-1}, respectively. The regions of high uncertainty were analogous to those between the methods (Figure S10).

Methodology for estimating SOC under future climate change

Among the five methods chosen for predicting SOC for the two soil layers in this study, RF and RFOK performed well in terms of prediction accuracy evaluation, SOC spatial distribution patterns, and model robustness (Note S2). Moreover, RF and RFOK had the strongest correlation (0.99 for SOC20 and ~1 for SOC100; Figure S29). Therefore, for compatibility with the forward feature selection (FFS) algorithm (CAST FFS)[54,55] and model parsimony, the RF algorithm was used for the subsequent analysis (FFSRF).

Environmental covariates, as indicators, enable both an estimation of actual SOC storage as well as predicting the SOC storage potential[56,57](Figures S30 and S31; Note S2). More accurate predictions can be achieved by integrating appropriate environmental covariates into the model. However, adding some inappropriate environmental covariates to the model may produce overfitting or may be counterproductive. Moreover, several key environmental variables (e.g., Temp, Pre, elevation, etc.) can explain most of the spatial variability of SOC at the regional/subcontinent scales.[58,59] Thus, we used FFS to select the ideal set of predictor variables for SOC20 and SOC100 predictions under future climate change (Figure S3; Table S1; see Note S2 for details). FFS was performed in R using the CAST package.[60] To do this, FFS first trains models using all possible pairs of two predictor variables. Among these initial models, the best one is kept. Based on this best model, the predictor variables are iteratively increased, and each of the remaining variables is tested for its improvement of the currently best model. The algorithm terminates if none of the remaining variables improves the model's performance when added to the current best model. More details about FFS are provided elsewhere.[54,55]

The results of the variable selection for FFS are shown in Note S2. Accordingly, we assumed that the variables remained constant over time, except for the climatic variables (i.e., annual Pre and mean annual Temp). This allowed us to obtain the climate-driven model. Based on this, spatial projections of SOC were performed under different climate-change scenarios. Future multi-scenario monthly Pre dataset and monthly mean Temp dataset (spatial resolution of ~1 km for the period January 2021 to December 2100), based on the IPCC Coupled Model Intercomparison Program Phase 6 (CMIP6), were obtained from the National Earth System Science Data Center, National Science & Technology Infrastructure of China (http://www.geodata.cn). Three SSPs are available: SSP119, SSP245, and SSP585. They represent the sustainable route, intermediate route, and fossil fuel development, respectively.[9]

Overall, this study developed a climate-driven approach, which allows projections using future climate-change scenario data (i.e., Temp and Pre) that are easily available. Consistent with previous studies[61] at the sub-continental scale, SOC storage is primarily determined by mean annual Temp, annual Pre, elevation, SOs, Li, drainage, and other factors (Table S1).

SUPPLEMENTAL INFORMATION

Supplemental information can be found online at https://doi.org/10.1016/j.crsus.2024.100179.

ACKNOWLEDGMENTS

This study was supported by the National Natural Science Foundation of China (U2243225), the Strategic Priority Research Program of the Chinese Academy of Sciences (XDA23070201), and the Fundamental Research Funds for the Central Universities in China (2023HHZX002).

AUTHOR CONTRIBUTIONS

J.W. and L.D. conceived the study, performed the analysis, and led the writing. S.L., C.P., Y.L., C.Y., C.T., S.P., B.W., and Z.S. helped with the results interpretation. J.W., J.L., and L.D. were responsible for data collection. All authors reviewed the manuscript and contributed to the manuscript writing.

DECLARATION OF INTERESTS

The authors declare no competing interests.

Received: July 2, 2024
Revised: July 13, 2024
Accepted: August 2, 2024
Published: August 28, 2024

REFERENCES

1. FAO; ITPS (2020). Global Soil Organic Carbon Map (GSOCmap). version 1.5: Technical report (FAO).
2. Schlesinger, W.H. (2005). Perspectives on Climate Change: Science, Economics, Politics, Ethics (Advances in the Economics of Environmental Resources, Vol. 5) (Emerald Group Publishing Limited), pp. 31–53.
3. Paustian, K., Collier, S., Baldock, J., Burgess, R., Creque, J., DeLonge, M., Dungait, J., Ellert, B., Frank, S., Goddard, T., et al. (2019). Quantifying carbon for agricultural soil management: from the current status toward a global soil information system. Carbon Manag. *10*, 567–587. https://doi.org/10.1080/17583004.2019.1633231.
4. Li, H.W., Wu, Y.P., Liu, S.G., Xiao, J.F., Zhao, W.Z., Chen, J., Alexandrov, G., and Cao, Y. (2022). Decipher soil organic carbon dynamics and driving forces across China using machine learning. Glob. Chang. Biol. *28*, 3394–3410. https://doi.org/10.1111/gcb.16154.
5. Deng, L., Liu, G.B., and Shangguan, Z.P. (2014). Land-use conversion and changing soil carbon stocks in China's 'Grain-for-Green' Program: a synthesis. Glob. Chang. Biol. *20*, 3544–3556. https://doi.org/10.1111/gcb.12508.
6. Li, J., and Heap, A.D. (2008). A Review of Spatial Interpolation Methods for Environmental Scientists*137* (Geoscience Australia). https://d28rz98at9flks.cloudfront.net/68229/Rec2008_023.pdf.
7. Hengl, T., Mendes de Jesus, J., Heuvelink, G.B.M., Ruiperez Gonzalez, M., Kilibarda, M., Blagotić, A., Shangguan, W., Wright, M.N., Geng, X.Y., Bauer-Marschallinger, B., et al. (2017). SoilGrids250m: global gridded soil information based on machine learning. PLoS ONE *12*, e0169748. https://doi.org/10.1371/journal.pone.0169748.
8. Liu, F., Wu, H.Y., Zhao, Y.G., Li, D.C., Yang, J.L., Song, X.D., Shi, Z., Zhu, A.X., and Zhang, G.L. (2022). Mapping high resolution National Soil

Information Grids of China. Sci. Bull. *67*, 328–340. https://doi.org/10.1016/j.scib.2021.10.013.

9. IPCC (2021). Climate Change 2021: The Physical Science Basis. Contribution of Working Group I to the Sixth Assessment Report of the Intergovernmental Panel on Climate Change (Cambridge University Press). https://doi.org/10.1017/9781009157896.002.
10. Yao, Y.T., Wang, X.H., Li, Y., Wang, T., Shen, M.G., Du, M.Y., He, H.L., Li, Y.N., Luo, W.J., Ma, M.G., et al. (2018). Spatiotemporal pattern of gross primary productivity and its covariation with climate in China over the last thirty years. Glob. Chang. Biol. *24*, 184–196. https://doi.org/10.1111/gcb.13830.
11. Peng, S.Z., Ding, Y.X., Liu, W.Z., and Li, Z. (2019). 1km monthly temperature and precipitation dataset for China from 1901 to 2017. Earth Syst. Sci. Data *11*, 1931–1946. https://doi.org/10.5194/essd-11-1931-2019.
12. Poggio, L., de Sousa, L.M., Batjes, N.H., Heuvelink, G.B.M., Kempen, B., Ribeiro, E., and Rossiter, D. (2021). SoilGrids 2.0: producing soil information for the globe with quantified spatial uncertainty. Soil *7*, 217–240. https://doi.org/10.5194/soil-7-217-2021.
13. Yang, R.M., Huang, L.M., Zhang, X., Zhu, C.M., and Xu, L. (2023). Mapping the distribution, trends, and drivers of soil organic carbon in China from 1982 to 2019. Geoderma *429*, 116232. https://doi.org/10.1016/j.geoderma.2022.116232.
14. Wang, J.J., Taylor, A.R., and D'Orangeville, L. (2023). Warming-induced tree growth may help offset increasing disturbance across the Canadian boreal forest. Proc. Natl. Acad. Sci. USA *120*, e2212780120. https://doi.org/10.1073/pnas.2212780120.
15. Wang, Z.G., Zhang, Y.Z., Govers, G., Tang, G.P., Quine, T.A., Qiu, J.X., Navas, A., Fang, H.Y., Tan, Q., and Van Oost, K.V. (2023). Temperature effect on erosion-induced disturbances to soil organic carbon cycling. Nat. Clim. Chang. *13*, 174–181. https://doi.org/10.1038/s41558-022-01562-8.
16. Xu, L., Yu, G.R., He, N.P., Wang, Q.F., Gao, Y., Wen, D., Li, S.G., Niu, S.L., and Ge, J.P. (2018). Carbon storage in China's terrestrial ecosystems: A synthesis. Sci. Rep. *8*, 2806. https://doi.org/10.1038/s41598-018-20764-9.
17. Mulder, V.L., Lacoste, M., Richer-de-Forges, A.C., and Arrouays, D. (2016). GlobalSoilMap France: High-resolution spatial modelling the soils of France up to two meter depth. Sci. Total Environ. *573*, 1352–1369. https://doi.org/10.1016/j.scitotenv.2016.07.066.
18. Walden, L., Serrano, O., Zhang, M., Shen, Z., Sippo, J.Z., Bennett, L.T., Maher, D.T., Lovelock, C.E., Macreadie, P.I., Gorham, C., et al. (2023). Multi-scale mapping of Australia's terrestrial and blue carbon stocks and their continental and bioregional drivers. Commun. Earth Environ. *4*, 189. https://doi.org/10.1038/s43247-023-00838-x.
19. Whittaker, R.H. (1962). Classification of natural communities. Bot. Rev. *28*, 1–239. https://doi.org/10.1007/BF02860872.
20. Yu, Z., Ciais, P., Piao, S.L., Houghton, R.A., Lu, C.Q., Tian, H.Q., Agathokleous, E., Kattel, G.R., Sitch, S., Goll, D., et al. (2022). Forest expansion dominates China's land carbon sink since 1980. Nat. Commun. *13*, 5374. https://doi.org/10.1038/s41467-022-32961-2.
21. Tang, X., Zhao, X., Bai, Y., Tang, Z., Wang, W., Zhao, Y., Wan, H., Xie, Z., Shi, X., Wu, B., et al. (2018). Carbon pools in China's terrestrial ecosystems: new estimates based on an intensive field survey. Proc. Natl. Acad. Sci. USA *115*, 4021–4026. https://doi.org/10.1073/pnas.1700291115.
22. Tifafi, M., Guenet, B., and Hatté, C. (2018). Large Differences in Global and Regional Total Soil Carbon Stock Estimates Based on SoilGrids, HWSD, and NCSCD: Intercomparison and Evaluation Based on Field Data From USA, England, Wales, and France. Global Biogeochemical Cycles *32*, 42–56. https://doi.org/10.1002/2017GB005678.
23. Shangguan, W., Dai, Y.J., Duan, Q.Y., Liu, B.Y., and Yuan, H. (2014). A global soil data set for earth system modeling. J. Adv. Model. Earth Syst. *6*, 249–263. https://doi.org/10.1002/2013MS000293.
24. Qiu, L.J., Yu, M.Z., Wu, Y.P., Yao, Y.Y., Wang, Z.S., Shi, Z.Y., and Guan, Y.H. (2021). Assessing and predicting soil carbon density in China using CMIP5 earth system models. Sci. Total Environ. *799*, 149247. https://doi.org/10.1016/j.scitotenv.2021.149247.
25. Dove, N.C., Torn, M.S., Hart, S.C., and Taş, N. (2021). Metabolic capabilities mute positive response to direct and indirect impacts of warming throughout the soil profile. Nat. Commun. *12*, 2089. https://doi.org/10.1038/s41467-021-22408-5.
26. Friedlingstein, P., Jones, M.W., O'Sullivan, M., Andrew, R.M., Bakker, D.C.E., Hauck, J., Le Quéré, C., Peters, G.P., Peters, W., Pongratz, J., et al. (2022). Global Carbon Budget 2021. Earth Syst. Sci. Data *14*, 1917–2005. https://doi.org/10.5194/essd-14-1917-2022.
27. Piao, S.L., He, Y., Wang, X.H., and Chen, F.H. (2022). Estimation of China's terrestrial ecosystem carbon sink: Methods, progress and prospects. Sci. China Earth Sci. *65*, 641–651. https://doi.org/10.1007/s11430-021-9892-6.
28. Wang, Y.L., Wang, X.H., Wang, K., Chevallier, F., Zhu, D., Lian, J.H., He, Y., Tian, H.Q., Li, J.S., Zhu, J.X., et al. (2022). The size of the land carbon sink in China. Nature *603*, E7–E9. https://doi.org/10.1038/s41586-021-04255-y.
29. Fang, J.Y., Yu, G.R., Liu, L.L., Hu, S.J., and Chapin, F.S. (2018). Climate change, human impacts, and carbon sequestration in China. Proc. Natl. Acad. Sci. USA *115*, 4015–4020. https://doi.org/10.1073/pnas.1700304115.
30. He, H.L., Wang, S.Q., Zhang, L., Wang, J.B., Ren, X.L., Zhou, L., Piao, S.L., Yan, H., Ju, W.M., Gu, F.X., et al. (2019). Altered trends in carbon uptake in China's terrestrial ecosystems under the enhanced summer monsoon and warming hiatus. Natl. Sci. Rev. *6*, 505–514. https://doi.org/10.1093/nsr/nwz021.
31. Xu, L., He, N.P., Li, M.X., Cai, W.X., and Yu, G.R. (2024). Spatiotemporal dynamics of carbon sinks in China's terrestrial ecosystems from 2010 to 2060. Resour. Conserv. Recycl. *203*, 107457. https://doi.org/10.1016/j.resconrec.2024.107457.
32. Wang, S., Bao, X.L., Feng, K., Deng, Y., Zhou, W.J., Shao, P.S., Zheng, T.T., Yao, F., Yang, S., Liu, S.E., et al. (2021). Warming-driven migration of core microbiota indicates soil property changes at continental scale. Sci. Bull. *66*, 2025–2035. https://doi.org/10.1016/j.scib.2021.01.021.
33. Liu, S.E., Sun, Z.L., Tian, P., Zhao, X.C., Zhou, G.Y., Dietrich, P., Wang, Q.K., and Delgado-Baquerizo, M. (2023). Temperature legacies predict microbial metabolic quotient across forest biomes. Global Ecol. Biogeogr. *32*, 107–119. https://doi.org/10.1111/geb.13609.
34. Wang, M.M., Guo, X.W., Zhang, S., Xiao, L.J., Mishra, U., Yang, Y.H., Zhu, B., Wang, G.C., Mao, X.L., Qian, T., et al. (2022). Global soil profiles indicate depth-dependent soil carbon losses under a warmer climate. Nat. Commun. *13*, 5514. https://doi.org/10.1038/s41467-022-33278-w.
35. Song, J., Wan, S.Q., Piao, S.L., Knapp, A.K., Classen, A.T., Vicca, S., Ciais, P., Hovenden, M.J., Leuzinger, S., Beier, C., et al. (2019). A meta-analysis of 1,119 manipulative experiments on terrestrial carbon-cycling responses to global change. Nat. Ecol. Evol. *3*, 1309–1320. https://doi.org/10.1038/s41559-019-0958-3.
36. Terrer, C., Phillips, R.P., Hungate, B.A., Rosende, J., Pett-Ridge, J., Craig, M.E., van Groenigen, K.J., Keenan, T.F., Sulman, B.N., Stocker, B.D., et al. (2021). A trade-off between plant and soil carbon storage under elevated CO_2. Nature *591*, 599–603. https://doi.org/10.1038/s41586-021-03306-8.
37. Francesca Cotrufo, M.F., Lavallee, J.M., Zhang, Y., Hansen, P.M., Paustian, K.H., Schipanski, M., and Wallenstein, M.D. (2021). In-N-Out: A hierarchical framework to understand and predict soil carbon storage and nitrogen recycling. Glob. Chang. Biol. *27*, 4465–4468. https://doi.org/10.1111/gcb.15782.
38. Crowther, T.W., Todd-Brown, K.E.O., Rowe, C.W., Wieder, W.R., Carey, J.C., Machmuller, M.B., Snoek, B.L., Fang, S., Zhou, G., Allison, S.D., et al. (2016). Quantifying global soil carbon losses in response to warming. Nature *540*, 104–108. https://doi.org/10.1038/nature20150.

39. Döscher, R., Acosta, M., Alessandri, A., Anthoni, P., Arsouze, T., Bergman, T., Bernardello, R., Boussetta, S., Caron, L.P., Carver, G., et al. (2022). The EC-Earth3 Earth System Model for the Climate Model Intercomparison Project 6. Geosci. Mod. Devel. Discuss. *15*, 2973–3020.

40. Ding, J.Z., Li, F., Yang, G.B., Chen, L.Y., Zhang, B.B., Liu, L., Fang, K., Qin, S.Q., Chen, Y.L., Peng, Y.F., et al. (2016). The permafrost carbon inventory on the Tibetan Plateau: a new evaluation using deep sediment cores. Glob. Chang. Biol. *22*, 2688–2701. https://doi.org/10.1111/gcb.13257.

41. Zhao, L., Wu, X.D., Wang, Z.W., Sheng, Y., Fang, H.B., Zhao, Y.H., Hu, G.J., Li, W.P., Pang, Q.Q., Shi, J.Z., et al. (2018). Soil organic carbon and total nitrogen pools in permafrost zones of the Qinghai-Tibetan Plateau. Sci. Rep. *8*, 3656. https://doi.org/10.1038/s41598-018-22024-2.

42. Dong, L.W., Sun, Y., Ran, J.Z., Hu, W.G., Ji, M.F., Du, Q.J., Xiong, J.L., Gong, H.Y., Yao, S.R., Adnan Akram, M.A., et al. (2022). Ecosystem organic carbon storage and their drivers across the drylands of China. CATENA *214*, 106280. https://doi.org/10.1016/j.catena.2022.106280.

43. Yang, Y.H., Mohammat, A., Feng, J.M., Zhou, R., and Fang, J.Y. (2007). Storage, patterns and environmental controls of soil organic carbon in China. Biogeochemistry *84*, 131–141. https://doi.org/10.1007/s10533-007-9109-z.

44. Nelson, D.W., and Sommers, L.E. (1996). Total Carbon, Organic Carbon, and Organic Matter. Methods of Soil Analysis. In Methods of Soil Analysis: Part II, Second Edition, A.L. Page, R.H. Miller, and D.R. Keeney, eds. (American Society of Agronomy), pp. 539–576.

45. Deng, L., Shangguan, Z., Bell, S.M., Soromotin, A.V., Peng, C., An, S., Wu, X., Xu, X., Wang, K., Li, J., et al. (2023). Carbon in Chinese grasslands: meta-analysis and theory of grazing effects. Carbon Res. *2*, 19. https://doi.org/10.1007/s44246-023-00051-7.

46. Jenny, H. (1994). Factors of Soil Formation: A System of Quantitative Pedology (McGraw-Hill).

47. McBratney, A.B., Mendonça Santos, M.L., and Minasny, B. (2003). On digital soil mapping. Geoderma *117*, 3–52. https://doi.org/10.1016/S0016-7061(03)00223-4.

48. Zuur, A.F., Ieno, E.N., and Elphick, C.S. (2010). A protocol for data exploration to avoid common statistical problems. Methods in Ecology and Evolution *1*, 3–14. https://doi.org/10.1111/j.2041-210X.2009.00001.x.

49. R Core Team (2020). R: A Language and Environment for Statistical Computing (R Foundation for Statistical Computing).

50. Cook-Patton, S.C., Leavitt, S.M., Gibbs, D., Harris, N.L., Lister, K., Anderson-Teixeira, K.J., Briggs, R.D., Chazdon, R.L., Crowther, T.W., Ellis, P.W., et al. (2020). Mapping carbon accumulation potential from global natural forest regrowth. Nature *585*, 545–550. https://doi.org/10.1038/s41586-020-2686-x.

51. Chen, S.C., Martin, M.P., Saby, N.P.A., Walter, C., Angers, D.A., and Arrouays, D. (2018). Fine resolution map of top- and subsoil carbon sequestration potential in France. Sci. Total Environ. *630*, 389–400. https://doi.org/10.1016/j.scitotenv.2018.02.209.

52. Alsamamra, H., Ruiz-Arias, J.A., Pozo-Vázquez, D., and Tovar-Pescador, J. (2009). A comparative study of ordinary and residual kriging techniques for mapping global solar radiation over southern Spain. Agr. For. Meteorol. *149*, 1343–1357. https://doi.org/10.1016/j.agrformet.2009.03.005.

53. Lin, L.I. (1989). A Concordance Correlation Coefficient to Evaluate Reproducibility. Biometrics *45*, 255–268. https://doi.org/10.2307/2532051.

54. Meyer, H., Reudenbach, C., Hengl, T., Katurji, M., and Nauss, T. (2018). Improving performance of spatio-temporal machine learning models using forward feature selection and target-oriented validation. Environ. Modell. Soft. *101*, 1–9. https://doi.org/10.1016/j.envsoft.2017.12.001.

55. Meyer, H., Reudenbach, C., Wöllauer, S., and Nauss, T. (2019). Importance of spatial predictor variable selection in machine learning applications – Moving from data reproduction to spatial prediction. Ecol. Modell. *411*, 108815. https://doi.org/10.1016/j.ecolmodel.2019.108815.

56. Sha, Z.Y., Bai, Y.F., Li, R.R., Lan, H., Zhang, X.L., Li, J., Liu, X.F., Chang, S.J., and Xie, Y.C. (2022). The global carbon sink potential of terrestrial vegetation can be increased substantially by optimal land management. Commun. Earth Environ. *3*, 1–10.

57. Bai, Y.F., and Cotrufo, M.F. (2022). Grassland soil carbon sequestration: current understanding, challenges, and solutions. Science *377*, 603–608. https://doi.org/10.1126/science.abo2380.

58. Chen, S.C., Arrouays, D., Leatitia Mulder, V.L., Poggio, L., Minasny, B., Roudier, P., Libohova, Z., Lagacherie, P., Shi, Z., Hannam, J., et al. (2022). Digital mapping of GlobalSoilMap soil properties at a broad scale: a review. Geoderma *409*, 115567. https://doi.org/10.1016/j.geoderma.2021.115567.

59. Wiesmeier, M., Urbanski, L., Hobley, E., Lang, B., von Lützow, M., Marin-Spiotta, E., van Wesemael, B., Rabot, E., Ließ, M., Garcia-Franco, N., et al. (2019). Soil organic carbon storage as a key function of soils - a review of drivers and indicators at various scales. Geoderma *333*, 149–162. https://doi.org/10.1016/j.geoderma.2018.07.026.

60. Meyer, H., Ludwig, M., Reudenbach, C., Nauss, T., and Pebesma, E. (2022). CAST: 'caret' Applications for Spatial-Temporal Models. GitHub. https://github.com/HannaMeyer/CAST.

61. Doetterl, S., Stevens, A., Six, J., Merckx, R., Oost, K.V., Pinto, M.C., Casanova-Katny, A., Muñoz, C., Boudin, M., Venegas, E.Z., and Boeckx, P. (2015). Soil carbon storage controlled by interactions between geochemistry and climate. Nat. Geosci. *8*, 780–783.